THE JOURNAL OF PHYSICAL CHEMISTRY B

Article

pubs.acs.org/JPCB

Probing Anisotropic Structure Changes in Proteins with Picosecond Time-Resolved Small-Angle X-ray Scattering

Hyun Sun Cho,[†] Friedrich Schotte,[†] Naranbaatar Dashdorj,[†] John Kyndt,[‡] and Philip A. Anfinrud*[,†]

[†]Laboratory of Chemical Physics, National Institute of Diabetes and Digestive and Kidney Diseases, National Institutes of Health, Bethesda, Maryland 20892, United States

[‡]College of Science and Technology, Bellevue University, Nebraska 68005, United States

ABSTRACT: We have exploited the principle of photoselection and the method of time-resolved small-angle X-ray scattering (SAXS) to investigate protein size and shape changes following photoactivation of photoactive yellow protein (PYP) in solution with ∼150 ps time resolution. This study partially overcomes the orientational average intrinsic to solution scattering methods and provides structural information at a higher level of detail. Photoactivation of the *p*-coumaric acid (pCA) chromophore in PYP produces a highly contorted, short-lived, red-shifted intermediate (pR_0), and triggers prompt, protein compaction of approximately 0.3% along the direction defined by the electronic transition dipole moment of the chromophore. Contraction along this dimension is accompanied by expansion along the orthogonal directions, with the net protein volume change being approximately −0.25%. More than half the strain arising from formation of pR_0 is relieved by the pR_0 to pR_1 structure transition (1.8 ± 0.2 ns), with the persistent strain presumably contributing to the driving force needed to generate the spectroscopically blue-shifted pB signaling state. The results reported here are consistent with the near-atomic resolution structural dynamics reported in a recent time-resolved Laue crystallography study of PYP crystals and suggest that the early time structural dynamics in the crystalline state carry over to proteins in solution.

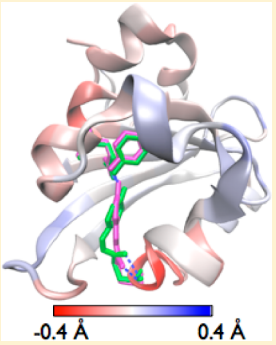

I. INTRODUCTION

Proteins are not static macromolecules, as depicted by their crystal structure. Rather, their structures are dynamic and can undergo conformational changes that modulate their function. To understand *how* a protein functions, it is crucial to know how its conformation evolves as it executes its function. The method of time-resolved Laue crystallography, first demonstrated on the nanosecond time scale by Moffat and coworkers,[1] was later extended to the picosecond time scale and used to literally watch a protein as it functions with near-atomic spatial resolution and 150 ps time resolution.[2] However, the structural changes observed in crystallographic studies are constrained by crystal packing, which may limit the range of motions accessible to the protein. For example, a recent 150 ps time-resolved Laue crystallography study of photoactive yellow protein (PYP) reported four transient intermediates in its photocycle, the last of which is the putative *precursor* of the signaling state.[3] The actual signaling state, which purportedly involves partial unfolding of the protein, is inaccessible within the confines of a protein crystal. Therefore, it is crucial to complement time-resolved crystallographic studies with structural studies of proteins in solution, where conformational changes can proceed free of the constraints imposed by crystal contacts.

Whereas time-resolved spectroscopic studies of proteins in solution can be quite sensitive to local structure changes involving a chromophore and/or its immediate environment, structural interpretation of transient spectra can be tenuous. The transient grating technique[4] extends the capabilities of time-resolved spectroscopy to the global scale and can be used to probe time-resolved changes in protein volume.[5] If one can properly account for the electronic contribution to the transient grating signal generated with parallel and perpendicular polarized laser pulses, this technique can also be used to probe anisotropic volume changes.[6] Nevertheless, the interpretation of these data is challenging, and its application to protein systems has not been widespread. On the other hand, small- and wide-angle X-ray scattering (SAXS/WAXS) patterns are encoded with structural information over a broad range of length scales, with the SAXS region providing incisive information about protein size and shape. Therefore, time-resolved SAXS/WAXS patterns of proteins in solution can provide structural information about transient intermediates that is complementary to time-resolved Laue crystallography.

The first nanosecond time-resolved X-ray scattering study of a protein focused on the WAXS region and reported time-dependent structural dynamics in hemoglobin.[7] To further advance this methodology, we developed on the BioCARS beamline at the Advanced Photon Source the infrastructure required to record time-resolved X-ray scattering patterns in both SAXS and WAXS regions simultaneously with ∼100 ps time resolution.[8] A recent time-resolved X-ray scattering study of PYP performed at the European Synchrotron Radiation

Special Issue: Michael D. Fayer Festschrift

Received: July 30, 2013
Revised: October 11, 2013
Published: October 14, 2013

Facility also demonstrated the ability to access both SAXS and WAXS regions;[9] however, the microsecond time resolution achieved in that study was too slow to examine the early structural dynamics in the PYP photocycle, which is the focus of this work.

PYP is a small (14 kD) blue-light receptor that has proven useful as a model system for probing structural dynamics in proteins.[3,9−14] This protein is found in *Halorhodospira halophila*,[15] a purple sulfur bacterium that swims away from blue light and toward photosynthetically useful green light.[16,17] The action spectrum for negative phototaxis matches the absorbance spectrum of PYP,[17] suggesting that this protein is responsible for the signal that causes this halophile to swim away from the UV end of the solar spectrum, which contains photons energetic enough to be genetically harmful. The chromophore in PYP is *p*-coumaric acid (pCA), which is covalently linked to the Cys69 residue of PYP via a thioester bond (Figure 1A). Upon absorbing a blue photon, the pCA

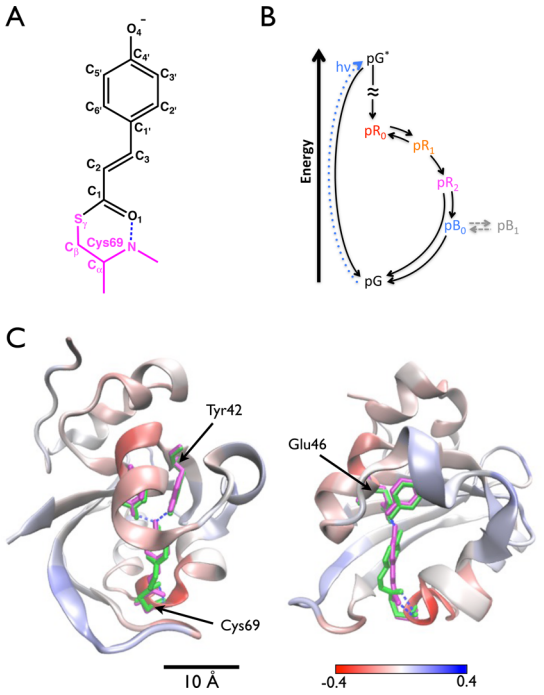

Figure 1. (A) The pCA chromophore absorbs blue light and gives PYP its yellow color. (B) Photoexcitation of PYP triggers trans-to-cis isomerization of the C_2═C_3 bond and launches a reversible photocycle that produces a transient PYP signaling state. (C) Front and side views of PYP in the pG (PDB ID: 2ZOH, magenta) and pR_0 (PDB ID: 4B9O, green) states, with atomic rendering of pCA and its hydrogen-bonding partners (Tyr42, Glu46, and Cys69). H-bonds are indicated with blue dashed lines. The protein is rendered as ribbon, which is color coded according to the Cα displacement accompanying the pG to pR_0 transition. Inward (red) and outward (blue) displacements relative to the PYP center of mass indicate compaction along the long axis of the pCA chromophore. Rendered with VMD (http://www.ks.uiuc.edu/Research/vmd/).

chromophore undergoes trans-to-cis isomerization,[18−22] an ultrafast event that triggers a reversible photocycle involving both red- and blue-shifted spectroscopic intermediates (Figure 1B), the last of which corresponds to the putative signaling state of PYP.[23−25]

The pCA chromophore is stabilized in its ground trans state by two unusually short and strong hydrogen bonds with Tyr42 and Glu46[26] and a third hydrogen bond between the pCA carbonyl and the Cys69 backbone nitrogen (see the magenta structure in Figure 1C). Of great interest is the molecular mechanism by which pCA photoisomerization drives the protein conformational changes that lead to the PYP signaling state. To explore this issue, two recent picosecond time-resolved Laue crystallography studies of PYP[3,11] attempted to extract from time-resolved electron density maps the structures of intermediates in the PYP photocycle. However, differences in the models employed in those studies led to conflicting views of the earliest intermediates. Kaila et al.[27] showed that the structures reported in Schotte et al.[3] are more consistent with both density functional theory and prior studies, and we summarize those results here. The photocycle reported in Schotte et al. involves four intermediates: pR_0, pR_1, pR_2, and pB_0 (see Figure 1B). The pCA chromophore in pR_0 was found in a strained cis conformation with its carbonyl oriented nearly perpendicular to the phenolate plane (see the green structure in Figure 1C). This highly contorted configuration appears to be engaged in a "tug of war" with torsional strain pulling the carbonyl toward a more planar pCA configuration, while its hydrogen bond with the Cys69 backbone nitrogen holds it back. Rupture of this hydrogen bond triggers the pR_0 to pR_1 transition and produces a planar cis pCA conformation. The dihedral angles on either side of the cysteine sulfur in pR_1 are found in a syn−syn conformation, suggesting intramolecular steric strain along the pCA backbone. This strain is relieved by the pR_1 to pR_2 transition (~16 ns), which converts these dihedrals to an anti−anti conformation via a bicycle-pedal motion about the Cys69 sulfur. The pR_2 state is the most stable red-shifted conformation and persists out to hundreds of microseconds. Photoisomerization-induced strain is evident not only in the pCA chromophore, but also in the protein backbone, whose atomic coordinates unveil distortion in the size and shape of PYP (see color-coded ribbon in Figure 1C). Indeed, the protein undergoes compaction along a direction defined by the long axis of the pCA chromophore. Evidently, the chromophore acts like a winch, with trans-to-cis photoisomerization creating strain in both the pCA and the surrounding protein.

Are the aforementioned crystallographic observations extensible to the solution phase, where PYP is free of the constraints imposed by crystal packing forces? To explore this possibility, we exploit the principle of photoselection[28,29] and the method of time-resolved SAXS to investigate protein size and shape changes following photoactivation of PYP in solution. Whereas the method of photoselection has long been used to extract orientational information in proteins[30−33] and was recently used to characterize anisotropy in the WAXS pattern of photolyzed MbCO,[34] the signatures recovered in prior studies do not directly assess protein size and shape, nor the directionality of such a change. Here, we record time-resolved SAXS scattering patterns with ~150 ps time resolution and show that photoactivation of PYP in solution triggers prompt protein compaction in a direction defined by the long axis of the chromophore. Moreover, we show that strain resulting from this structural change persists out to long time scales and presumably provides the driving force needed to generate the PYP signaling state.

II. EXPERIMENTAL SECTION

Functionally active holo-PYP was produced biosynthetically in *Escherichia coli* using a dual plasmid system, with one expressing

dx.doi.org/10.1021/jp407593j | J. Phys. Chem. B 2013, 117, 15825−15832

PYP from *H. halophila*, and the other expressing a two-gene operon consisting of tyrosine ammonia lyase and *p*-hydroxycinnamic acid ligase.[35] After isolation and purification, PYP was concentrated to ~50 mg·mL^{-1} and dialyzed against 150 mM NaCl, 20 mM sodium phosphate buffer, pH 6.

Picosecond time-resolved SAXS/WAXS "snapshots" of PYP were acquired on the BioCARS 14-ID-B beamline at the Advanced Photon Source (APS) using the pump−probe method.[8] Briefly, a laser "pump" pulse photoactivated PYP confined inside a capillary, after which its 2D scattering pattern was recorded with a suitably delayed, high fluence X-ray "probe" pulse isolated from the APS hybrid mode (Figure 2).

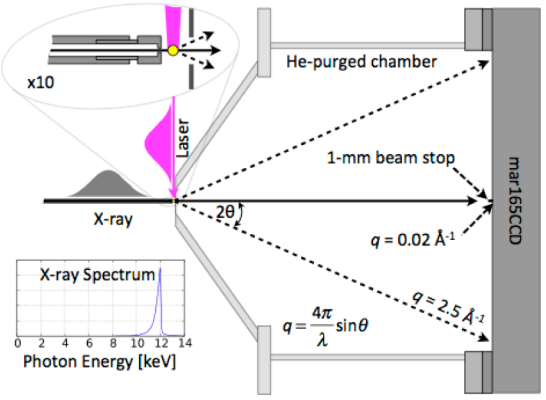

Figure 2. Experimental geometry used to acquire time-resolved X-ray scattering data. The protein solution (~50 mg·mL^{-1} protein in a 20 mM sodium phosphate buffer at pH 6.0 with 150 mM NaCl) is contained in a ~0.6 mm diameter thin-wall fused silica capillary. The laser pulse (~100 ps fwhm; 390 nm) is directed downward and focused to an elliptical spot (120 × 600 μm; ~2.5 mJ·mm^{-2}) with the long axis parallel to the X-ray direction of propagation. The X-ray pulse (~117 ps fwhm; ~80 μm; ~1.4 × 10^{10} photons/pulse) passes through the center of the capillary, continues through a helium-purged chamber, and is absorbed by a 1 mm diameter tungsten beam stop. The asymmetric X-ray spectrum is sharply peaked at 12 keV and has a bandwidth of ~320 eV (2.7% fwhm). Scattered X-rays are detected on a mar165CCD detector over a range of q spanning 0.02 Å^{-1} to beyond 2.5 Å^{-1}.

For this study, the sample temperature was maintained at 22 °C with a high-precision temperature controller. After each pump−probe pair, the capillary was translated 240 μm along a direction orthogonal to the X-ray and laser beams. The 25-mm stroke of the linear translation stage permitted accumulation of 100 pump−probe pairs per stroke at a repetition frequency of 41 Hz. The X-ray imaging detector integrated up to 11 strokes (1100 X-ray pulses) before reading the image. This move−stop−acquire approach provided ample time for the sample to recover from photoexcitation and spread the radiation dose over a larger volume. After acquiring each image, a syringe pump pushed fresh sample into the interaction region of the capillary. The 2D scattering images were reduced to 1D curves in which the scattering intensity, I (photons/pixel), was computed as a function of the scattering vector magnitude $q = (4\pi \sin\theta)/\lambda$, where 2θ is the scattering angle and λ is the wavelength of the incident X-ray beam in Å. Time-resolved scattering differences were generated by subtracting scattering curves acquired without laser excitation from those acquired with laser excitation. The time resolution achievable with the pump−probe method is determined by the convolution of the pump and probe pulses, which was about 150 ps fwhm in this study.

The SAXS/WAXS patterns recorded consist of photons scattered from the buffer, glass capillary, helium, and protein, with the protein accounting for about 5% of the total number of photons detected. Since the pump-induced change in the protein scattering pattern is at the few percent level, the signal of interest is typically at the 10^{-4}−10^{-3} level, requiring repeated measurements to attain the statistical precision needed to characterize time-dependent changes in the protein structure. The scattering differences reported here represent the average of up to 18 repeated measurements. Furthermore, singular value decomposition (SVD) was employed to filter the data and improve the signal-to-noise ratio (S/N) of the 1D scattering curves.

The relatively low single-photon quantum efficiency for photoisomerization of pCA in PYP limits the S/N achievable in time-resolved X-ray scattering studies.[13] To boost the yield, the protein solution was photoexcited with intense, 390 nm, circularly polarized laser pulses stretched to 100 ps. This pulse duration is long compared to the excited state lifetime of ~1−3 ps,[18−22] which affords the protein multiple opportunities to photoisomerize during the excitation pulse, and thereby enhances the overall photoisomerization yield. Because the cis isomer of pCA has a red-shifted absorption spectrum, excitation on the blue side of the ground state absorption spectrum (absorbance maximum: 446 nm) is more favorable as it minimizes the probability that a single chromophore absorbs more than one photon during the excitation pulse. Since the 100 ps laser pulse duration is short compared to the protein tumbling time of ~10 ns, only about 1/3 of the protein molecules have a pCA dipole orientation favorable for photoexcitation with a linearly polarized laser pulse. By converting the excitation polarization from linear to circular, the yield is improved by nearly a factor of 2.

III. RESULTS AND DISCUSSION

It is well-known that small-angle X-ray scattering is sensitive to particle size and shape. SAXS is a contrast method whose forward scattering intensity, $I(q = 0)$, is proportional to the square of the number of excess electrons in a particle relative to an equivalent volume of its surroundings:[36]

$$I(q = 0) \propto (\Delta n_e)^2 = (\Delta\rho)^2 V^2 \quad (1)$$

where the number of excess electrons Δn_e has been expressed in terms of the electron density difference between a particle and its surroundings $(\Delta\rho)$ and the volume of the particle (V). In vacuum, any change in particle volume is compensated by its corresponding change in density, so the forward scattering intensity is independent of size and shape and depends only on the number of electrons. For particles in solution, the density difference term overwhelms the corresponding change in volume, making the forward scattering intensity quite sensitive to changes in particle volume. A change in particle volume can be triggered by structural changes within the particle, by association with other particles, or by particle dissociation. For example, if light absorption triggers expansion of a protein in solution, its electron density decreases, causing the contrast between the protein and surrounding solvent electron densities $(\Delta\rho)$ to diminish. The accompanying decrease in the integrated scattering power of the main SAXS scattering feature can be used to quantify the corresponding change in protein volume.

dx.doi.org/10.1021/jp407593j | J. Phys. Chem. B 2013, 117, 15825−15832

For example, time-resolved SAXS differences following photolysis of MbCO unveiled a prompt ~0.7% decrease in the integrated SAXS intensity,[8] which according to eq 1, corresponds to a volume change of +0.1% (calculation assumes the integral of $q{\cdot}I$ over the main SAXS feature is proportional to $I(q = 0)$, the protein volume is 21.6×10^3 Å^3, and the electron densities for buffer and MbCO are, respectively, 0.337 and 0.431 e$^-$/Å^3).

Time-resolved SAXS difference curves acquired following photoactivation of PYP are shown in Figure 3A. To put the

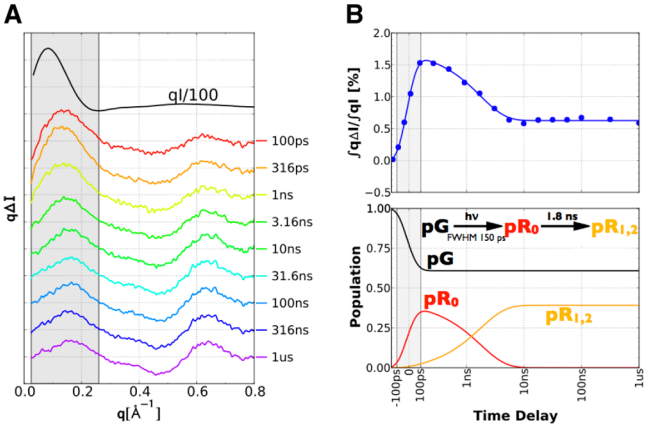

Figure 3. Time-resolved X-ray scattering of PYP. (A) SAXS differences recorded as a function of pump−probe time delay ($q\Delta I$: light on minus light off). For clarity, only a subset of the data acquired are shown. For comparison, the static scattering pattern of PYP in its ground state is shown ($qI/100$; black line). (B) Top: Time dependence of the integrated SAXS intensity (integral over the shaded region in panel A). The experimental data (filled circles) are fitted with a population-based kinetic model (line). The time axis is linear in the shaded region and logarithmic elsewhere. Bottom: Two-state sequential model used to interpret the time-dependence of the integrated SAXS intensity. The time axis is linear in the shaded region and logarithmic elsewhere. The time-dependent populations of pR_0 and $pR_{1,2}$ were computed assuming a pR_0 yield of 0.4 and an instrument response function of 153 ps fwhm. The growth of pR_0 tracks the integral of the instrument response function, and its transition to $pR_{1,2}$ proceeds with a least-squares-determined lifetime of 1.8 ns.

difference curves on the same relative scale as the static curve, they were extrapolated from 40% to 100% photoactivation. The time dependence of the integrated SAXS intensity, shown in Figure 3B, was divided by the ground state amplitude to compute the relative change. This curve is well-described by a prompt, instrument-response-limited rise, followed by a single exponential relaxation to a long-lived state. The prompt, ~1.8% *increase* in the integrated SAXS intensity corresponds to a volume change of −0.25%. The fact that this signal develops in a direction opposite that observed following photolysis of MbCO is convincing evidence that the change in integrated SAXS intensity arises from a structural change, not a thermal effect, and corresponds to light-induced protein contraction.

At the relatively high protein concentration employed in this study (50 mg·mL^{-1}), the absolute scattering amplitude in the SAXS region is attenuated due to the packing structure factor, $S(q)$. Though this structure factor need not be the same for the ground and photoactivated states of PYP, any evolution would likely track the rotational diffusion dynamics of PYP in solution. Therefore, by recording SAXS patterns on a time scale that is short compared to rotational diffusion and calculating *relative* changes in the scattering power, we avoid the complications that arise from structure factor issues while benefiting from the S/N improvement afforded with elevated protein concentrations.

To assess whether the magnitude of protein compaction is sensible, we determined the crystallographic volume change from the atomic coordinates for the ground (pG) and first intermediate (pR_0) states of PYP according to $\Delta V/V = 3\Delta r/r$, where r refers to the RMS distance of the atoms relative to the center of mass of the protein. The crystallographic volume change was found to be −0.28%, which is very similar to the −0.25% change determined from our time-resolved SAXS study. The volume change found for I_T (PDB 4I38), the first PYP intermediate recently reported by Jung et al.,[11] was found to be −0.38%. Since the authors of that work did not specify the ground state structure used to generate their difference maps, we performed this calculation assuming our ground state structure, which may introduce systematic error into this estimate. The fact that the crystallographic and solution determinations for pR_0 are similar suggests that the structural changes observed at high resolution in the crystal are extensible to the solution phase.

We interpret the time dependence of the integrated SAXS intensity with a sequential two-state kinetic model (Figure 3B) that is a simplified version of a kinetic model used to interpret time-resolved Laue diffraction data.[3] Photoisomerization of pCA produces pR_0, a strained cis intermediate whose formation triggers contraction of the protein (Figure 1C) and a concomitant increase in the integrated SAXS intensity. The resulting strain in the protein is partially relieved by a structure transition occurring with a lifetime of 1.8 ± 0.2 ns (Figure 3B). Due to the similarity between our 1.8 ± 0.2 ns lifetime and ~1−3 ns lifetimes reported in time-resolved spectroscopic studies of PYP,[18−20,22] we assign this relaxation to the pR_0 to pR_1 transition. Note that these lifetimes are somewhat longer than the ~0.6 ns lifetime reported for pR_0 in a time-resolved crystallography study of PYP.[3] However, that lifetime is shortened by the unavoidable <30 K adiabatic temperature jump that arises when photoactivating optically dense PYP crystals (~55 mM) with high power density (~3.5 mJ·mm^{-2}) laser pulses.

According to time-resolved Laue crystallography,[3] the pR_1 to pR_2 transition occurs with a rate of (~16 ns)$^{-1}$. However, we find no direct evidence for a transition on this time scale in the integrated SAXS intensity (Figure 3B), which remains relatively constant from 10 ns to 1 μs. Time-resolved optical studies have not reported spectroscopic changes on this time scale either. One possible explanation for these observations is that pR_1 and pR_2 are indistinguishable spectroscopically and in SAXS. The pR_1 to pR_2 structure transition has been characterized as a bicycle-pedal dihedral angle rotation involving atoms on either side of the cysteine sulfur.[3] Since this motion would not disturb π conjugation in the pCA chromophore, it would not be surprising if this structural change was spectroscopically silent. Moreover, if the pR_1 to pR_2 transition were volume-conserving, it would not be observable in time-resolved SAXS. Alternatively, it is possible that the transition from pR_1 to pR_2 proceeds promptly in the solution phase, with the observed 1.8 ns time constant corresponding to the appearance of pR_2. Regardless, the fact that the change in integrated SAXS intensity remains positive after formation of $pR_{1,2}$ demonstrates that PYP remains in a contracted state, with the persistent

dx.doi.org/10.1021/jp407593j | J. Phys. Chem. B 2013, 117, 15825−15832

strain presumably required to drive PYP into the pB_1 signaling state on a much longer time scale.

As illustrated in Figure 4A, the pCA chromophore in PYP preferentially absorbs light polarized along its long axis.

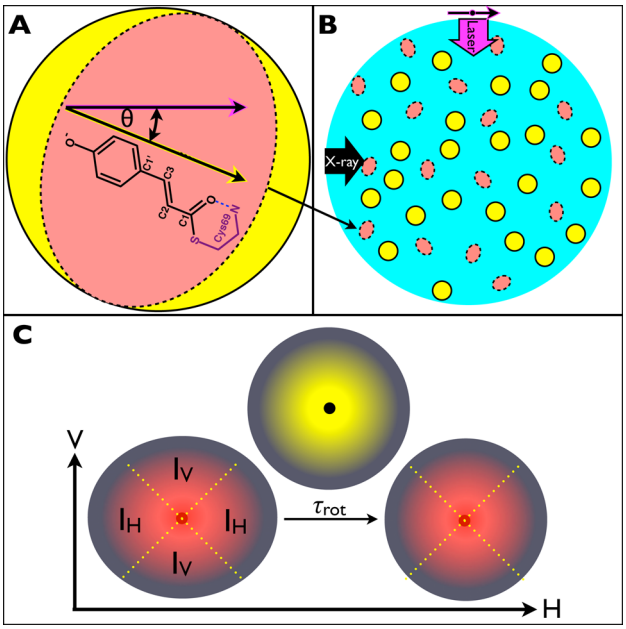

Figure 4. Photoselection of PYP in solution. (A) The absorption probability of the pCA chromophore is proportional to $\cos^2\theta$, where θ is the angle between the laser polarization vector (magenta arrow) and the transition dipole moment for pCA (yellow arrow), which is nominally aligned along the pCA long axis. Photoisomerization of pCA triggers protein contraction, with the resulting red-shifted intermediate (pR_0) depicted as a red ellipsoid. (B) With the orthogonal pump–probe geometry employed, photoactivation of PYP produces an anisotropic orientational distribution of pR_0 that favors PYP whose pCA is aligned with the laser polarization vector. The photoisomerization yield in this cartoon depiction of a 200 Å thick slab of ~50 mg·mL^{-1} protein is 40%. (C) Scattering from an anisotropic orientational distribution of pR_0 intermediates can produce an anisotropic X-ray scattering pattern: contraction of the protein along the laser polarization direction broadens the X-ray scattering distribution in the horizontal direction. Rotational diffusion erases the anisotropy generated by polarized laser excitation.

Therefore, polarized laser excitation of PYP produces an anisotropic distribution of photoactivated protein molecules (Figure 4B). Since we employ an orthogonal pump–probe geometry with the laser beam directed downward (Figure 2), the photoactivated intermediates will be nominally aligned with the pCA chromophore axis pointing in the horizontal direction. This result is true for either linear or circular polarized laser excitation. The resulting anisotropic distribution of pR_0 intermediates should produce an anisotropic X-ray scattering pattern, whose vertical (I_V) and horizontal (I_H) contributions differ (Figure 4C). To record these differences, the time resolution of the measurement must be fast compared to the rotational tumbling time for PYP in aqueous solution.

Because the anisotropic scattering differences (I_H–I_V) recorded at early time delays are about an order of magnitude weaker than the ~10^{-2} pump-induced change in the scattering intensities, the signal-to-noise ratio for individual time-resolved anisotropic scattering patterns is rather poor. Consequently, we report in Figure 5A the average of time-resolved anisotropic

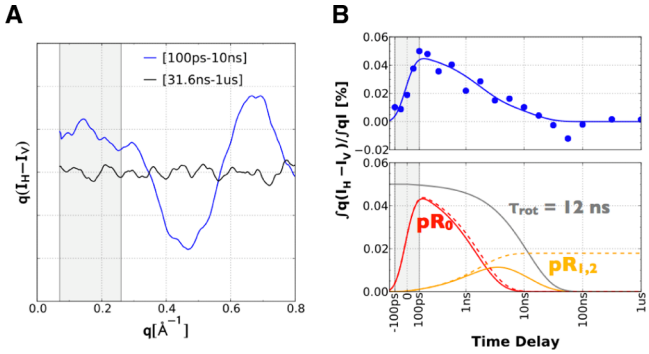

Figure 5. Anisotropic SAXS scattering. (A) Horizontal minus vertical scattering differences, $q(I_H-I_V)$, averaged for pump–probe time delays from 50 ps to 10 ns (blue), and from 31.6 ns to 1 μs (black). The scattering curves were smoothed with a sigma-weighted 0.1 Å^{-1} wide moving average. (B) Top: Time dependence of the (I_H-I_V) difference recorded in the SAXS region (shaded region in panel A). The experimental data (filled circles) are well-described (solid line) by a sequential two-state kinetic model that includes rotational tumbling. The time axis is linear in the shaded region and logarithmic elsewhere. Bottom: Time dependence of the pR_0 (red) and $pR_{1,2}$ (orange) contributions to the (I_H-I_V) difference were computed with (solid lines) and without (dashed lines) rotational tumbling. The overall anisotropic scattering signal decays exponentially (gray) with a rotational tumbling time constant of 12 ns.

scattering patterns acquired at positive time delays before (blue) and after (black) rotational tumbling destroys this anisotropy. According to a time-resolved fluorescence anisotropy measurement, the rotational diffusion time for PYP at low concentration is 7.8 ns.[37] Therefore, we used the 17.8 ns time point as the separator for this grouping. As expected the anisotropy is absent in the long-time average. The early time average, on the other hand, exhibits features in both SAXS (shaded) and WAXS regions. Since the SAXS signal is more readily interpreted, we focus on that region.

As shown in Figure 5B, the integral of $q(I_H-I_V)$ over the main SAXS feature rises promptly and appears to decay biexponentially. Because we expect the pR_0 to pR_1 transition to reduce the magnitude of this difference, we fixed the rate constant for this transition to the value recovered from the decay of the integrated SAXS intensity shown in Figure 3B. The remaining fit parameters were refined via Levenberg–Marquardt nonlinear least-squares. The 12 ± 3 ns time constant recovered for rotational diffusion is somewhat slower than the 7.8 ns time constant recovered from time-resolved fluorescence anisotropy measurements.[37] However, our time-resolved SAXS/WAXS study was conducted at relatively high protein concentration, which increases the viscosity of the solution and slows rotational diffusion. For example, the rotational diffusion time constant reported for human hemoglobin at low protein concentration, ~26–35 ns,[38−40] is somewhat faster than the ~46 ns time constant recovered from a time-resolved absorbance study of hemoglobin conducted at ~60 mg·mL^{-1} (Cho, unpublished data). Assuming PYP behaves similarly, the 12 ns rotational diffusion time recovered at 50 mg·mL^{-1} is not inconsistent with the 7.8 ns diffusion time reported at low concentration.

The fact that the SAXS scattering at early times is brighter in the horizontal than vertical direction demonstrates quite clearly that light-induced PYP contraction is nominally aligned with the horizontal polarization direction of the exciting laser pulse.

dx.doi.org/10.1021/jp407593j | J. Phys. Chem. B 2013, 117, 15825−15832

Therefore, time-resolved SAXS measurements are not only capable of quantifying volume changes associated with a light-induced structure transition, but when recorded on time scales short compared to rotational diffusion, can be extended to determine the directionality of this dimensional change relative to the molecular frame.

Because the photoexcitation probability is proportional to $\cos^2\theta$, where θ is the angle between the laser polarization and the transition dipole of the chromophore, the maximum degree of photoselection achievable when photoactivating an isotropic distribution of chromophores with linearly polarized light at low fluence is 3:1 (ratio of parallel to perpendicular oriented populations). When photoactivating a significant fraction of the population, the degree of photoselection diminishes even further due to saturation effects. Since our aim was not to maximize the degree of photoselection but instead maximize the total population of PYP entering into its reversible photocycle, we photoactivated the protein with high fluence circularly polarized laser pulses. Circularly polarized light can be decomposed into two orthogonal components of equal amplitude, with one component producing a 3:1 anisotropic distribution of photoexcited molecules (horizontal to vertical) and the other a 1:1 distribution. Their combined effect reduces the degree of photoselection to 2:1. The excited population oriented along the X-ray propagation direction does not contribute to the $(I_H - I_V)$ difference. In this study, circular polarized excitation with 390 nm, 2.5 mJ·mm^{-2}, ∼100 ps pulses photoactivated approximately 40% of the protein in the volume probed by the X-ray beam and produced an anisotropic scattering difference $\sim 10^{-3}$ times the absolute scattering intensity. Although the degree of photoselection and the magnitude of the measured anisotropic signal would have been larger with linearly polarized excitation, the signal recorded proved large enough to unambiguously determine the nominal direction of the protein compaction relative to the pCA transition moment.

Protein contraction in one dimension should be accompanied by expansion along the two orthogonal directions, with the overall protein volume change dependent on their relative magnitudes. If we assume the same degree of expansion along the two orthogonal directions, it is possible to relate the measured anisotropic scattering difference to changes in protein dimension parallel (Δa) and perpendicular (Δb) to the pCA transition dipole moment. Since contraction in one dimension increases the integrated SAXS scattering power along that dimension, it is sensible to assume the early time anisotropic scattering difference in Figure 5B is proportional to the difference $(\Delta a/a - \Delta b/b)$. Therefore, we need only find the proportionality constant to determine the relative dimensional changes. To that end, we computed the theoretical scattering differences that arise when compressing spheres into oblate ellipsoids and used numerical simulations to calculate their orientational distribution given our laser excitation conditions (∼40% photoexcitation with circular polarization). From this numerical simulation, we found that a −1% change in the difference $(\Delta a/a - \Delta b/b)$ produces an anisotropic scattering difference of 0.112%. Therefore, our experimentally determined difference of 0.048% for pR_0 corresponds to the difference $(\Delta a/a - \Delta b/b) \approx -0.43\%$. Given our experimental determination for the protein volume change, $\Delta V/V = -0.25\%$ and the relationship between volumetric and dimensional changes, $\Delta V/V = \Delta a/a + 2\Delta b/b$, we find the following solutions: $\Delta a/a = -0.37\%$ and $\Delta b/b = 0.06\%$. Note that decomposition of the protein volume change into components parallel $(\Delta a/a)$ and perpendicular $(\Delta b/b)$ to the pCA transition moment is sensitive to systematic errors in their relative magnitude. Moreover, the assumption that protein expansion orthogonal to the pCA transition moment can be described by a single parameter, $\Delta b/b$, is admittedly crude. Nevertheless, it is fruitful to compare results from this analysis with the crystallographically determined anisotropic structure change that accompanies the pG to pR_0 transition. For this calculation, we assumed the pCA transition moment is aligned along the long axis of the chromophore and computed the change of the second moments of all non-hydrogen protein atom coordinates along the direction parallel $(\Delta a/a = -0.67\%)$ and perpendicular $(\Delta b/b = 0.27\%)$ to its long axis. Though not in quantitative agreement, the fact that the SAXS determination for $\Delta a/a$ is within a factor of 2 of the Laue determination suggests that picosecond time-resolved SAXS can be used to not only assess time-resolved changes in protein volume, but when recorded on time scales fast compared to rotational diffusion, can also unveil the directionality of protein expansion/contraction.

During the 1.8 ns pR_0 to pR_1 transition, both the PYP scattering power (Figure 3B) and its anisotropic scattering difference (Figure 5B) decrease to ∼37% their original amplitudes. This observation suggests that the global protein structure responds to the pR_0 to pR_1 transition in an elastic and reversible fashion and provides additional support for our hypothesis that the pCA chromophore acts like a winch and induces strain that helps drive the conformational changes that lead to the PYP signaling state.

IV. CONCLUSIONS

Our time-resolved SAXS study of PYP following polarized photoactivation has unveiled photoisomerization-induced compaction of the protein along the long axis of the pCA chromophore. By exploiting the principle of photoselection, we have partially overcome the orientational average intrinsic to solution scattering methods and thereby obtained structural information at a higher level of detail. Photoisomerization of pCA promptly creates strain in PYP, which partially relaxes during the ∼1.8 ns pR_0 to $pR_{1,2}$ transition. The time-dependent change in protein volume demonstrates that neither photoisomerization of the pG state nor relaxation of pR_0 to $pR_{1,2}$ are volume-conserving structure transitions, at least not on a global scale. The strain that persists after formation of pR_1 presumably helps drive the conformational changes that lead to the PYP signaling state. The results reported here are consistent with the near-atomic resolution structural dynamics reported in a time-resolved Laue crystallography study of PYP[3] and suggest that the early time structural dynamics in the crystalline state carry over to proteins in solution. The fact that the integrated SAXS signal grows promptly demonstrates that ∼150 ps time resolution is not adequate to track the development of the observed protein compaction. However, the rate at which this structural change develops could be recorded at a free electron X-ray laser facility such as the Linac Coherent Light Source (LCLS) in Stanford, CA.

AUTHOR INFORMATION

Corresponding Author

*Phone: 301-435-6034. E-mail: anfinrud@nih.gov.

Present Address
N.D.: Onom, Inc., 65 Abrams Court, Stanford, CA 94305, United States.

Notes
The authors declare no competing financial interest.

■ ACKNOWLEDGMENTS

We thank Dr. Rob Henning and Dr. Irina Kosheleva for assistance preparing the 14-ID-B beamline for our studies and Bernard Howder, Jr. for machining many of the components required to pursue time-resolved x-ray studies on this beamline. We are grateful to the late Prof. Cusanovich for his early participation in this collaborative effort. Use of the BioCARS Sector 14 was supported by National Center for Research Resources Grant 5P41RR007707 and National Institute of General Medical Sciences Grant 8P41GM103543 from NIH. Use of the Advanced Photon Source, an Office of Science User Facility operated for the U.S. Department of Energy (DOE) Office of Science by Argonne National Laboratory, was supported by U.S. DOE Contract DE-AC02-06CH11357. The time-resolved setup at Sector 14 was funded in part through collaboration with P.A.A. This research was supported by the Intramural Research Program of the National Institute of Diabetes and Digestive and Kidney Diseases, NIH. VMD was developed by the Theoretical and Computational Biophysics Group in the Beckman Institute for Advanced Science and Technology at the University of Illinois at Urbana−Champaign.

■ REFERENCES

(1) Srajer, V.; Teng, T. Y.; Ursby, T.; Pradervand, C.; Ren, Z.; Adachi, S.; Schildkamp, W.; Bourgeois, D.; Wulff, M.; Moffat, K. Photolysis of the Carbon Monoxide Complex of Myoglobin: Nanosecond Time-Resolved Crystallography. *Science* **1996**, *274* (5293), 1726−1729.

(2) Schotte, F.; Lim, M. H.; Jackson, T. A.; Smirnov, A. V.; Soman, J.; Olson, J. S.; Phillips, G. N.; Wulff, M.; Anfinrud, P. A. Watching a Protein as it Functions with 150-ps Time-resolved X-ray Crystallography. *Science* **2003**, *300* (5627), 1944−1947.

(3) Schotte, F.; Cho, H. S.; Kaila, V. R.; Kamikubo, H.; Dashdorj, N.; Henry, E. R.; Graber, T. J.; Henning, R.; Wulff, M.; Hummer, G.; et al. Watching a Signaling Protein Function in Real Time via 100-ps Time-resolved Laue Crystallography. *Proc. Natl. Acad. Sci. U.S.A.* **2012**, *109* (47), 19256−61.

(4) Salcedo, J. R.; Siegman, A. E.; Dlott, D. D.; Fayer, M. D. Dynamics of Energy Transport in Molecular Crystals: The Picosecond Transient-Grating Method. *Phys. Rev. Lett.* **1978**, *41* (2), 131−134.

(5) Goodno, G. D.; Miller, R. J. D. Femtosecond Heterodyne-Detected Four-Wave-Mixing Studies of Deterministic Protein Motions. 1. Theory and Experimental Technique of Diffractive Optics-Based Spectroscopy. *J. Phys. Chem. A* **1999**, *103* (49), 10619−10629.

(6) Goodno, G. D.; Astinov, V.; Miller, R. J. D. Femtosecond Heterodyne-detected four-wave-mixing Studies of Deterministic Protein Motions. 2. Protein Response. *J. Phys. Chem. A* **1999**, *103* (49), 10630−10643.

(7) Cammarata, M.; Levantino, M.; Schotte, F.; Anfinrud, P. A.; Ewald, F.; Choi, J.; Cupane, A.; Wulff, M.; Ihee, H. Tracking the Structural Dynamics of Proteins in Solution using Time-resolved wide-angle X-ray Scattering. *Nat. Methods* **2008**, *5* (10), 881−6.

(8) Cho, H. S.; Dashdorj, N.; Schotte, F.; Graber, T.; Henning, R.; Anfinrud, P. Protein Structural Dynamics in Solution Unveiled via 100-ps Time-resolved X-ray Scattering. *Proc. Natl. Acad. Sci. U.S.A.* **2010**, *107* (16), 7281−6.

(9) Kim, T. W.; Lee, J. H.; Choi, J.; Kim, K. H.; van Wilderen, L. J.; Guerin, L.; Kim, Y.; Jung, Y. O.; Yang, C.; Kim, J.; et al. Protein Structural Dynamics of Photoactive Yellow Protein in Solution Revealed by Pump-Probe X-ray Solution Scattering. *J. Am. Chem. Soc.* **2012**, *134* (6), 3145−3153.

(10) Ihee, H.; Rajagopal, S.; Srajer, V.; Pahl, R.; Anderson, S.; Schmidt, M.; Schotte, F.; Anfinrud, P. A.; Wulff, M.; Moffat, K. Visualizing Reaction Pathways in Photoactive Yellow Protein from Nanoseconds to Seconds. *Proc. Natl. Acad. Sci. U.S.A.* **2005**, *102* (20), 7145−7150.

(11) Jung, Y. O.; Lee, J. H.; Kim, J.; Schmidt, M.; Moffat, K.; Srajer, V.; Ihee, H. Volume-conserving trans-cis isomerization Pathways in Photoactive Yellow Protein Visualized by Picosecond X-ray Crystallography. *Nat. Chem.* **2013**, *5* (3), 212−20.

(12) Tripathi, S.; Srajer, V.; Purwar, N.; Henning, R.; Schmidt, M. pH Dependence of the Photoactive Yellow Protein Photocycle Investigated by Time-Resolved Crystallography. *Biophys. J.* **2012**, *102* (2), 325−332.

(13) Hellingwerf, K. J.; Hendriks, J.; Gensch, T. Photoactive Yellow Protein, a new type of Photoreceptor Protein: Will this "yellow lab" bring us where we want to go? *J. Phys. Chem. A* **2003**, *107* (8), 1082−1094.

(14) Imamoto, Y.; Kataoka, M. Structure and Photoreaction of Photoactive Yellow Protein, a Structural Prototype of the PAS Domain Superfamily. *Photochem. Photobiol.* **2007**, *83* (1), 40−49.

(15) Meyer, T. E. Isolation and Characterization of Soluble Cytochromes, Ferredoxins and Other Chromophoric Proteins from the Halophilic Phototrophic Bacterium Ectothiorhodospira-Halophila. *Biochim. Biophys. Acta* **1985**, *806* (1), 175−183.

(16) Hustede, E.; Liebergesell, M.; Schlegel, H. G. The Photophobic Response of Various Sulfur and Nonsulfur Purple Bacteria. *Photochem. Photobiol.* **1989**, *50* (6), 809−815.

(17) Sprenger, W. W.; Hoff, W. D.; Armitage, J. P.; Hellingwerf, K. J. The Eubacterium Ectothiorhodospira-Halophila Is Negatively Phototactic, with a Wavelength Dependence That Fits the Absorption-Spectrum of the Photoactive Yellow Protein. *J. Bacteriol.* **1993**, *175* (10), 3096−3104.

(18) Ujj, L.; Devanathan, S.; Meyer, T. E.; Cusanovich, M. A.; Tollin, G.; Atkinson, G. H. New photocycle intermediates in the Photoactive Yellow Protein from Ectothiorhodospira halophila: Picosecond transient Absorption Spectroscopy. *Biophys. J.* **1998**, *75* (1), 406−412.

(19) Imamoto, Y.; Kataoka, M.; Tokunaga, F.; Asahi, T.; Masuhara, H. Primary Photoreaction of Photoactive Yellow Protein Studied by Subpicosecond-nanosecond spectroscopy. *Biochemistry* **2001**, *40* (20), 6047−6052.

(20) Larsen, D. S.; van Stokkum, I. H. M.; Vengris, M.; van der Horst, M. A.; de Weerd, F. L.; Hellingwerf, K. J.; van Grondelle, R. Incoherent Manipulation of the Photoactive Yellow Protein Photocycle with Dispersed pump-dump-probe Spectroscopy. *Biophys. J.* **2004**, *87* (3), 1858−1872.

(21) van Wilderen, L. J. G. W.; Van der Horst, M. A.; van Stokkum, I. H. M.; Hellingwerf, K. J.; van Grondelle, R.; Groot, M. L. Ultrafast Infrared Spectroscopy r\Reveals a Key Step for Successful Entry into the Photocycle for Photoactive Yellow Protein. *Proc. Natl. Acad. Sci. U.S.A.* **2006**, *103* (41), 15050−15055.

(22) Heyne, K.; Mohammed, O. F.; Usman, A.; Dreyer, J.; Nibbering, E. T. J.; Cusanovich, M. A. Structural Evolution of the Chromophore in the Primary Stages of trans/cis isomerization in Photoactive Yellow Protein. *J. Am. Chem. Soc.* **2005**, *127* (51), 18100−18106.

(23) Meyer, T. E.; Yakali, E.; Cusanovich, M. A.; Tollin, G. Properties of a Water-Soluble, Yellow Protein Isolated from a Halophilic Phototrophic Bacterium that has Photochemical Activity Analogous to Sensory Rhodopsin. *Biochemistry* **1987**, *26* (2), 418−23.

(24) Meyer, T. E.; Tollin, G.; Hazzard, J. H.; Cusanovich, M. A. Photoactive Yellow Protein from the Purple Phototrophic Bacterium, Ectothiorhodospira-Halophila - Quantum Yield of Photobleaching and Effects of Temperature, Alcohols, Glycerol, and Sucrose on Kinetics of Photobleaching and Recover. *Biophys. J.* **1989**, *56* (3), 559−564.

(25) Meyer, T. E.; Tollin, G.; Causgrove, T. P.; Cheng, P.; Blankenship, R. E. Picosecond Decay Kinetics and Quantum Yield of Fluorescence of the Photoactive Yellow Protein from the Halophilic

Purple Phototrophic Bacterium, Ectothiorhodospira-Halophila. *Biophys. J.* **1991**, *59* (5), 988−991.
(26) Anderson, S.; Crosson, S.; Moffat, K. Short hydrogen bonds in Photoactive Yellow Protein. *Acta Crystallogr., D* **2004**, *60*, 1008−1016.
(27) Kaila, V. R.; Schotte, F.; Cho, H. S.; Hummer, G.; Anfinrud, P. Reconciling Contradictions in Time-resolved x-ray Structures of early Intermediates in the Photocycle of Photoactive Yellow Protein. *Nat. Chem.*, in press.
(28) Ansari, A.; Szabo, A. Theory of photoselection by Intense Light Pulses. Influence of Reorientational Dynamics and Chemical Kinetics on Absorbance Measurements. *Biophys. J.* **1993**, *64* (3), 838−51.
(29) Lakowicz, J. R. *Principles of fluorescence spectroscopy*, 3rd ed.; Springer: New York, 2006; p xxvi.
(30) Ansari, A.; Jones, C. M.; Henry, E. R.; Hofrichter, J.; Eaton, W. A. Photoselection in Polarized Photolysis Experiments on Heme Proteins. *Biophys. J.* **1993**, *64* (3), 852−68.
(31) Lim, M.; Jackson, T. A.; Anfinrud, P. A. Binding of CO to Myoglobin from a Heme Pocket Docking site to form nearly Linear Fe-C-O. *Science* **1995**, *269* (5226), 962−6.
(32) Lim, M.; Jackson, T. A.; Anfinrud, P. A. Ultrafast Rotation and Trapping of Carbon Monoxide Dissociated from Myoglobin. *Nat. Struct. Biol.* **1997**, *4* (3), 209−14.
(33) Moore, J. N.; Hansen, P. A.; Hochstrasser, R. M. Iron-carbonyl bond Geometries of Carboxymyoglobin and Carboxyhemoglobin in Solution Determined by Picosecond Time-resolved Infrared Spectroscopy. *Proc. Natl. Acad. Sci. U.S.A.* **1988**, *85* (14), 5062−6.
(34) Kim, J.; Kim, K. H.; Kim, J. G.; Kim, T. W.; Kim, Y.; Ihee, H. Anisotropic Picosecond X-ray Solution Scattering from Photoselectively Aligned Protein Molecules. *J. Phys. Chem. Lett.* **2011**, *2* (5), 350−356.
(35) Kyndt, J. A.; Vanrobaeys, F.; Fitch, J. C.; Devreese, B. V.; Meyer, T. E.; Cusanovich, M. A.; Van Beeumen, J. J. Heterologous Production of Halorhodospira halophila holo-photoactive Yellow Protein through Tandem Expression of the Postulated Biosynthetic Genes. *Biochemistry* **2003**, *42* (4), 965−970.
(36) Porod, G. General Theory. In *Small Angle X-ray Scattering*; Glatter, O.; Kratky, O., Eds.; Academic Press, Inc.: New York, 1982; pp 17−51.
(37) Otto, H.; Hoersch, D.; Meyer, T. E.; Cusanovich, M. A.; Heyn, M. P. Time-resolved Single tryptophan Fluorescence in Photoactive Yellow Protein Monitors Changes in the Chromophore Structure during the Photocycle via Energy Transfer. *Biochemistry* **2005**, *44* (51), 16804−16816.
(38) Jones, C. M.; Ansari, A.; Henry, E. R.; Christoph, G. W.; Hofrichter, J.; Eaton, W. A. Speed of Intersubunit Communication in Proteins. *Biochemistry* **1992**, *31* (29), 6692−702.
(39) McCalley, R. C.; Shimshick, E. J.; McConnell, H. M. Effect of Slow Rotational Motion on Paramagnetic-Resonance Spectra. *Chem. Phys. Lett.* **1972**, *13* (2), 115.
(40) Hofrichter, J.; Henry, E. R.; Szabo, A.; Murray, L. P.; Ansari, A.; Jones, C. M.; Coletta, M.; Falcioni, G.; Brunori, M.; Eaton, W. A. Dynamics of the Quaternary Conformational change in Trout Hemoglobin. *Biochemistry* **1991**, *30* (26), 6583−98.